The International Journal of Advanced Manufacturing Technology (2023) 126:163–178
https://doi.org/10.1007/s00170-023-11136-3

ORIGINAL ARTICLE

Influence of aging treatments on 17–4 PH stainless steel parts realized using material extrusion additive manufacturing technologies

Alessandro Pellegrini[1] · **Fulvio Lavecchia**[1] · **Maria Grazia Guerra**[1] · **Luigi Maria Galantucci**[1]

Received: 3 October 2022 / Accepted: 16 February 2023 / Published online: 23 February 2023

Abstract
The most relevant criticalities of parts produced by material extrusion additive manufacturing technologies are lower mechanical properties than standard material performances, the presence of pores caused by the manufacturing method, and issues related to the interface between layers and rods. In this context, heat treatments can be considered an effective solution for tailoring the material behavior to different application fields, especially when using precipitation hardening stainless steels. In this work, aging treatments were conducted on parts realized using three different extrusion-based processes: Atomic Diffusion Additive Manufacturing, bound metal deposition, and fused filament fabrication. Two conditions of direct aging (H900 and H1150) were considered with the aim of comparing the response of properties in the opposite conditions of peak-aged and overaged. The hardness tests revealed that H900 aging significantly influenced hardness (max increase of 52%), and porosity (− 34.3% with respect to the as-sintered condition). On the other hand, the H1150 aging decreased the hardness (− 18% max) and porosity (− 32.2% max). Substantial differences among the microstructures due to grain size and δ-ferrite were illustrated. A statistical test was included to better highlight the influence of the heat treatment on the investigated properties.

Keywords Additive manufacturing · Material extrusion · 17–4 PH stainless steel · Aging treatment · Hardness · Porosity

1 Introduction

Precipitation-hardened (PH) 17–4 PH (AISI 630) is a fully martensitic stainless steel when it is fabricated through conventional methods such as forging, casting, or welding [1]. Among other precipitate stainless steels, 17–4 PH is one of the most common, thanks to its main characteristics, such as high mechanical strength, hardness, and corrosion resistance, allowing a wide range of applications in automotive, aerospace, mechanical, and biomedical engineering [2]. It contains approximately 3–5 wt.% of copper (Cu), indeed, the high mechanical properties derive from a combination of the martensitic microstructure and the formation of sub-micron Cu-rich precipitates. The Cu-rich precipitates are generated during specific well-known post-process heat treatments, which can be tailored to change the precipitates size, shape, and hardness and strength of the post-processed components [3]. Additionally, on heat treated 17–4 PH, Cr-rich and Nb-rich precipitates are observed, but also Mn-, Ni-, and Si-rich phases may occur [4].

The 17–4 PH stainless steel can be processed by several powder-based additive manufacturing (AM) technologies, particularly laser powder-bed fusion (L-PBF), direct metal laser sintering (DMLS), direct energy deposition (DED), and by metal injection molding (MIM). More recently, other technologies such as, Binder Jetting 3D Printing (BJ3DP), and material extrusion additive manufacturing (MEX) [5] have been adopted for stainless steels. These latter belong to the "MIM-like" AM processes featuring similarities in metal powder characteristics, the use of a polymeric binder, and the Debinding and Sintering phases (D&S), necessary for obtaining a full metal part [6]. Thus, compared to the traditional Metal AM technologies, BJ3DP and MEX processes require a longer processing time to fabricate a solid metal part due to the oversizing of the part and the D&S phases necessary to remove the polymeric binder and to sinter the metal powder. Despite this, they are cheaper than direct processes in initial investments, equipment, low material wastage [7], and an easy operating system, reasonable control on processing parameters, and skilled labor [8].

✉ Alessandro Pellegrini
alessandro.pellegrini@poliba.it

[1] Department of Mechanical, Mathematic and Management Engineering, Polytechnic of Bari, Bari, Italy

The use of 17–4-PH by MEX technologies is common in literature [9–15] for the analysis of mechanical properties (tensile and yield strength, elastic modulus, hardness, flexural, and compression strength), relative density, roughness, and microstructural investigation. These characteristics are mainly influenced by the feedstock material composition, 3D printing parameters, debinding, and sintering methods and parameters.

The main characteristic of precipitation hardenable stainless steels is the possibility to heat treat them and modify their mechanical properties. According to this statement, in this paper, the effects of two different heat treatments were investigated on 17–4 PH specimens realized using three different MEX technologies.

1.1 State of art

Typical heat treatments on precipitation hardened stainless steels are reported in the standard ASTM A564 [16], where the temperature and holding time are varied according to the required condition. Possible heat treatments for precipitation-hardened stainless steels, as 17–4 PH, are solution-heat treatment (SHT) generally at 1040 °C for 30–40 min and subsequent aging with different times and temperatures or, alternately, only aging ("direct aging"). The heat treatments allow modifying the material mechanical properties and the material density [17].

In literature, there are several works regarding SHT followed by subsequently aging, or direct aging on as-built 17–4 PH. These works are mainly related to L-PBF technologies. One of the main investigated aspects is the correlation between different types of powder atomization (argon-Ar, nitrogen-N_2, or water) and the response of the material after the heat treatment. Meredith et al. [3] compared microhardness values of Ar-atomized powder and N_2-atomized powder heat treated with direct aging and SHT + aging at different temperatures and holding times. Murr et al. [18], evaluated the hardness values for the H900 parts comparing Ar and N_2 atomized powders and different printing shielding atmospheres (Ar and N_2). LeBrun et al. [19] evaluated mechanical properties varying the heat treatments temperatures and holding times in accordance with the material standard [16]. In [20], the investigation of the effect on the mechanical properties and microstructure of 17–4 PH parts of different post treatments—the direct aging, hot isostatic pressure (HIP) plus direct aging, SHT plus aging, and HIP plus SHT plus aging—was presented. The comparison between the H900 condition and SHT + H900, evaluating the effect on microstructure, percentage fractions of martensite and retained austenite, and on mechanical properties, was conducted [21]. The tensile and fatigue behavior of specimens H900 and H1025 aged with and without SHT was discussed by Nezhadfar et al. [22]. On the matrix, after SHT, was observed a microstructure completely martensitic and full of Cu-precipitates, responsible of the improve of hardness. Shaffer et al. [23] are using computational thermodynamic calculations in order to predict the effect of standard heat treatments on the mechanical properties of AM-fabricated materials, particularly those produced using laser-based PBF processes. Zhou et al. [24] revealed on the microstructure of 17–4 PH-aged specimens an increase of strength and hardness due to the precipitation of Cu during aging treatment. A prevalence dispersion occurred at interface of δ-ferrite and retained austenite. Chae et al. [25] investigated the principal strengthening factors that occur after aging or SHT + aging. Cu-precipitates dispersed randomly on the matrix had increase the yield strength of vertical and horizontal specimens. Particular attention has been paid on the feedstock and the presence of retained austenite. Huber et al. [26], on BJ parts, observed how after the SHT + H900 the structure is composed by ferrite and martensite and a part of retained austenite, compared to the as-sintered state where only martensite was found. The increase of temperature, the presence of copper precipitates, and reverted austenite were also considered in previous work on solutioned bars in 17–4 PH [27–29]. It should be noted that all the reported works on 17–4-PH heat treatments are mainly related to L-PBF and BJ3DP.

Heat treatments of MEX parts can be a solution for improving the mechanical characteristics or adjusting the material properties according to the required application, widening the implementation of these technologies for the fabrication of structural parts. In this context, there are very few studies dealing with heat treatments and its effects on MEX parts; furthermore, the adoption of post treatments with the aim to edit the properties of as-sintered parts is still not deepened. The aging treatments on 17–4 PH specimens manufactured using the proprietary system of Markforged Inc., the Atomic Diffusion Additive Manufacturing (ADAM), were reported in previous studies [30, 31]. Condruz et al. [30] quenched (1040 °C for 40 min) and tempered the specimens at different temperatures (450 °C and 550 °C) to evaluate the effects on the hardness and microstructure. However, the phases identified were not well presented. Bouaziz et al. [31] evaluated the surface roughness, tensile strength, and elongation of specimens as-sintered and treated with H900. A comparison between as-sintered state and SHT + H900 condition specimens in 17–4 PH (60 vol.%) manufactured via fused filament fabrication (FFF) showed an increase of the tensile strength and a decrease of porosity after the aging treatment [32].

The aim of this work is to understand how aging affects some properties of parts made by MEX. The direct aging method was selected as heat treatment, and it was conducted on the 17–4 PH steel parts manufactured with three different MEX technologies: Atomic Diffusion Additive

Manufacturing (ADAM), Bound Metal Deposition (BMD), and fused filament fabrication (FFF). Previous studies have shown that, after the printing, debinding, and sintering phases, the microstructures of parts made with the ADAM, BMD, and FFF (BASF feedstock) processes were different from each other and different from those observed on a forged 17–4 PH [15, 28, 32]. Thus, the effects of aging treatment are not certain, considering differences in feedstock, debinding, and sintering of MEX processes.

The SHT condition was not considered due to the sintering temperatures and time, which are sufficient to enable the complete solutioning of the material. In order to consider and investigate the opposite conditions of the material, two aging conditions were chosen, the peak-aged one, H900, and overaged one, H1150. Hardness and porosity were analyzed comparing the as-sintered and the heat-treated conditions. Using a scanning electron microscope were detected the precipitates that may occur after the heat treatment, and a statistical analysis was used to discuss the results obtained.

2 Material and methods

2.1 Materials and MEX technologies

In this paper, the martensitic 17–4 PH stainless steel was processed by three different MEX technologies: the first two, ADAM and BMD, are developed by two companies, Markforged Inc. and Desktop Metal Inc., respectively. Each of these companies provides their 17–4 PH feedstock, in the form of a mixture of a polymeric binder and metal powder with different volume percentages [33]. For BMD 17–4 PH, the percentage is approximately 60% [34], while the feedstock used for ADAM is a proprietary blend of polypropylene (2–4%), paraffin, and hydrocarbon waxes (2–6%), and the remaining is powder of 17–4 PH stainless steel [35]. The third technology was FFF, and the machine used to print 17–4 PH BASF Ultrafuse® material was Ultimaker S5. 17–4 PH BASF Ultrafuse® material is composed by a metal powder percentage of around 88%, and the remaining 12% is polyoxymethylene and polypropylene.

These three technologies consist of three main phases: printing, debinding, and sintering (PDS). More in detail, ADAM and FFF are referred as "filament-based" techniques. The filament, collected in a spool, is extruded by a heated nozzle on a heated building plate. While, the process patented by Desktop Metal Inc., called Bound Metal Deposition ™ (BMD), is defined "plunger-based" [36]. The feedstock used is shaped into rods having a well-defined and controlled diameter and housed in a specially designed and padded dispensing cartridge. During the printing process, the rods are pushed, by a plunger, in a heated extruder to produce a quasi-molten composite. This composite, extruded through a calibrated nozzle, is deposited on the building plate following a predetermined path to produce the part [14].

The printing parameters for ADAM and BMD are governed and predefined from proprietary slicer of each technology. In both systems, a heated nozzle of 0.40 mm and a heated platform were used. The FFF main printing parameters can be varied thanks to the use of an open slicer software. Printing speed at 35 mm/s, flow rate equal to 104%, 245 °C for nozzle with a diameter of 0.40 mm, and 130 °C for bed temperature were chosen. The 3D printing strategy was two perimetral lines, defined as "wall layers," a building orientation on the XY plan, a line infill pattern with raster angle of +/−45°, and an infill density of 100%. The specimens realized for the study presented a square area of 20 mm × 20 mm and a thickness of 3 mm.

As for the MIM, after the printing of the composite part, called "green part," the D&S process is required. This process allows to remove the polymeric binder through different methods and different sintering

Table 1 Summary table of the three different technologies [13, 34, 35, 37]

Phase		Technology		
		ADAM	BMD	FFF
Printing	Feedstock	Filament	Rods	Filament
	Metal powder (vol.%)	≃90	60	≃88
	Nozzle size	0.40 mm	0.25–0.40 mm	≥0.40 mm
Debinding	Method	Solvent	Solvent + Thermal	Catalytic
	Parameters	50 °C in Opteon SF79 fluid (4.1% mass loss)	*Solvent*: in a proprietary solvent (3–5% mass loss) *Thermal*: 350 °C-1 h and 450 °C-1 h in H_2 + 3% Ar atmosphere	120 °C-8 h in HNO_3 atmosphere
Sintering	Parameters	1100 °C-26/27 h in Ar + 3% H_2 atmosphere	1300–1370 °C-up to 2 h in Ar + 3% H_2 atmosphere	600 °C-1 h and 1300 °C-3 h in 100% clean and dry H_2 or Ar atmosphere

Table 2 Chemical composition of 17–4 PH stainless steel for each supplier

Material	Element (wt.%)				
	Cr	Ni	Cu	Mn	Si
Markforged	17.28 ± 0.20	3.71 ± 0.17	6.07 ± 0.54	0.73 ± 0.11	0.20 ± 0.06
BASF ultrafuse	16.22 ± 0.19	4.29 ± 0.18	5.73 ± 0.53	0.44 ± 0.11	0.37 ± 0.07
Desktop metal	17.09 ± 0.17	3.80 ± 0.15	4.96 ± 0.45	1.03 ± 0.12	0.67 ± 0.06
ASTM A564[16]	15–17.5	3.00–5.00	3.00–5.00	1.00	1.00

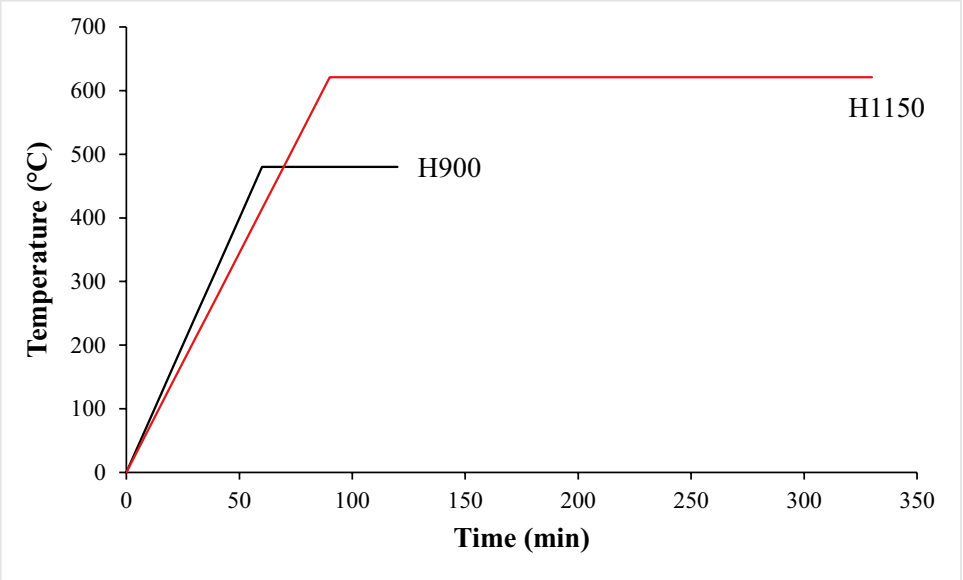

Fig. 1 Temperature profile for H900 and H1150 conditions

parameters obtaining the metal part. In Table 1, a summary of the main characteristics of the three technologies grouped by the printing debinding and sintering steps is reported.

The process parameters used for this work in D&S phase was the same reported in Table 1. Through energy dispersive X-ray spectrometry (EDS) analysis at scanning electron microscope (SEM), the chemical compositions on as-sintered condition are reported for the three different feedstocks in Table 2.

2.2 Heat treatment processes

For the heat treatment process, a conventional furnace with a maximum temperature of 800 °C was used. According to the standard ASTM A564, the aging condition of H900 requires a pre-heating of the chamber furnace up to 480 °C, a holding time of 1 h, and after a cooling in air. The H1150 aging condition, instead, requires a pre-heating up to 620 °C, a holding time of 4 h, and a cooling in air. The temperature profiles are showed in Fig. 1.

2.3 Pre- and post-treatment analysis

The pre- and post-treated specimens were analyzed considering the hardness and the porosity.

The Rockwell C hardness (HRC) test was conducted using the durometer (Ernst NR3D, Cisam-Ernst s.r.l., Italy) with a cone diamond penetrator with an opening angle of 120° and a load of 1471 N. Five replications were considered for each specimen (pre-aging and post-aging). The mean values and deviation standards were always considered for this study.

Table 3 Hardness values for the as-sintered specimens pre-H900 and pre-H1150 aging conditions. The data sheet values are received from each data sheet [37, 39, 40]

Technology	Hardness (HRC) before heat treatment		
	Pre-H900	Pre-H1150	Data sheet values
ADAM	32.8 ± 1.2	34.3 ± 0.9	30.0
BMD	24.4 ± 0.6	24.3 ± 0.5	26.0
FFF	27.2 ± 2.0	29.3 ± 1.2	32.2

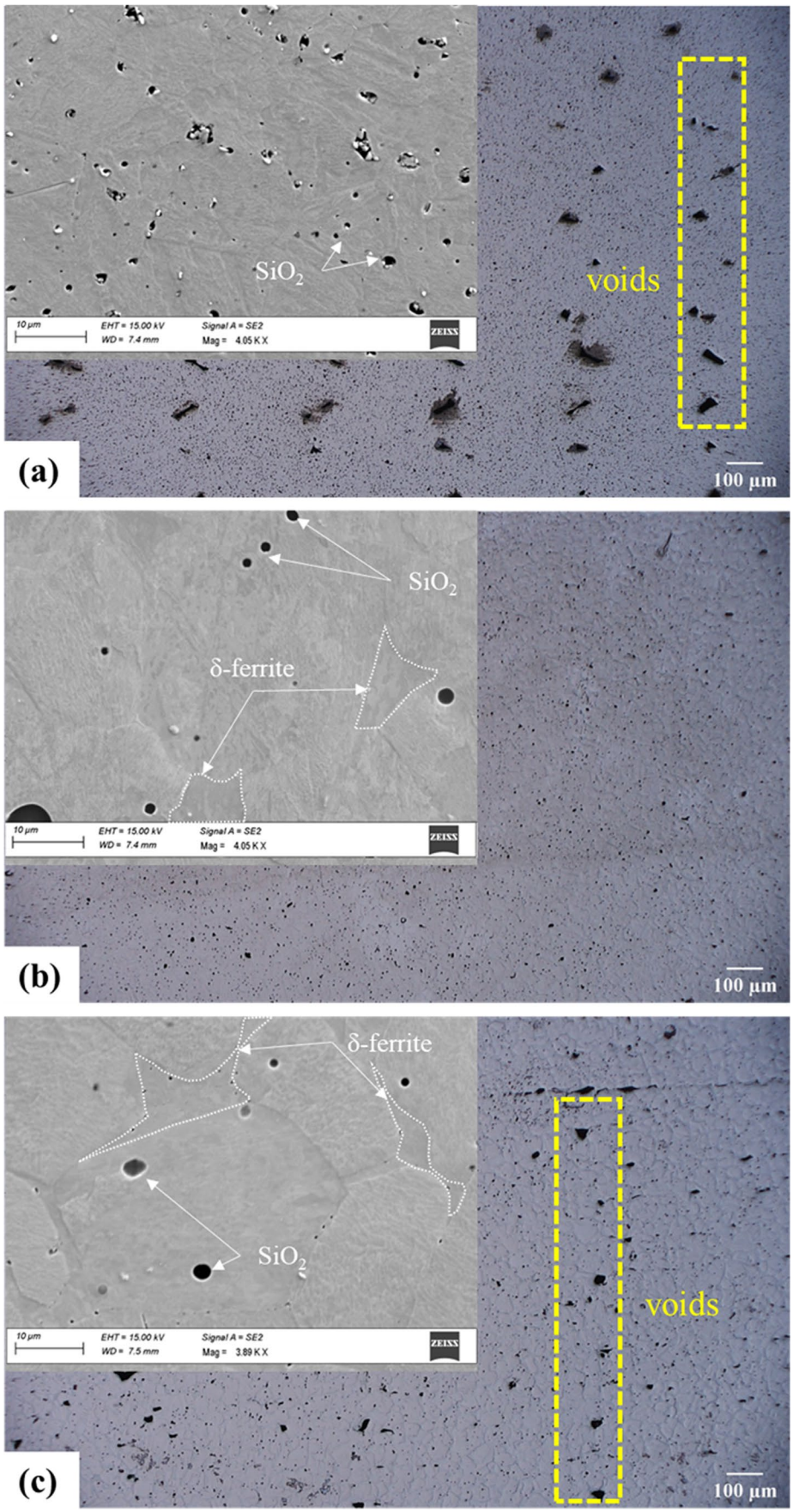

Fig. 2 Cross sections parallel to the building orientation of specimens realized observed at OM and SEM via (**a**) ADAM, (**b**) BMD, and (**c**) FFF

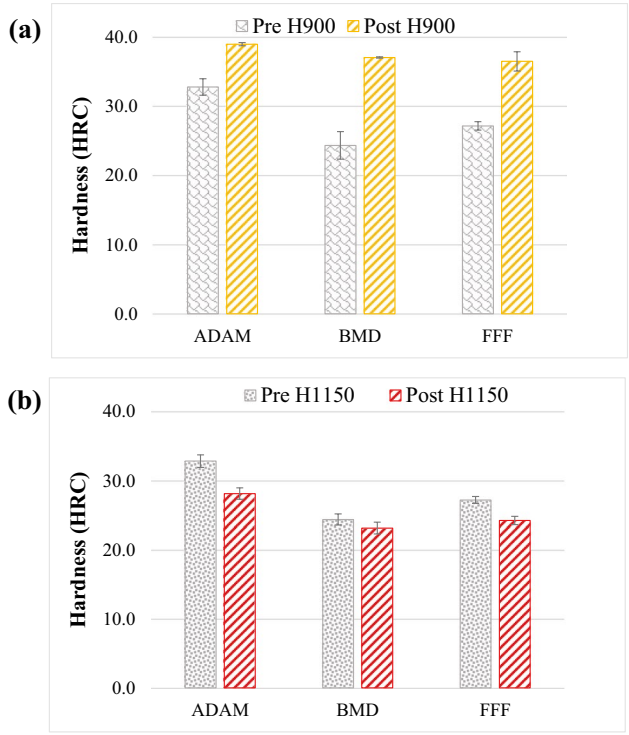

Fig. 3 Comparison of hardness for (**a**) pre-H900 and post-H900 (**b**) pre-H1150 and post-H1150

For the porosity evaluation, firstly, the traditional metallographic preparation was executed (cutting, grinding, and polishing) on as-sintered and aged specimens. Cross sections parallel to the building orientation were considered and observed with the optical microscope (OM) (Hirox RH-2000, Hirox Co., Ltd, Japan) with the "OL-140II" lens. Cross-sectional images were acquired and processed through the software ImageJ (http://imagej.nih.gov/ij/) to determine the porosity. To analyze the effect of heat treatment on the same material processed by ADAM, BMD, and FFF, at a more detailed level, the same specimens were observed at SEM (Sigma 300VP, Carl Zeiss AG, Germany) and (LEO EVO-50XVP, Zeiss, Cambridge, Cambridgeshire, UK). SEM was coupled with an X-max (80 mm^2) Silicon drift Oxford detector (Oxford Instruments, High Wycombe, Buckinghamshire, UK) equipped with a Super Atmosphere Thin Window ©. SEM operative conditions were 15-kV accelerating potential, 200-pA probe current and X-ray spectrum ED acquisition, about 25,000 output cps as average count rate on the whole spectrum, counting time 50 s, and 8.5-mm working distance. A final aperture of 30 µm was selected for cutting the electron beam.

The ED X-ray detector is positioned on the SEM column with 35° take-off angle and 35-mm working distance. The software for SEM control is SmartSEM, and the software for ED Oxford detector control is AZtec, both granted as software programs by Oxford-Link Analytical (U.K.) SEM–EDS operative conditions are also detailed in Mangone et al. [38]. The Marble's reagent solution (4 g CuSO4, 20 ml HCl, 40 ml H_2O) was used to identify the microstructures of as-sintered and aged specimens. Moreover, a statistical analysis of the mean was conducted utilizing a two-sample *t* test with significance level (α) of 0.05 to evaluate the effect of the aging on the two properties investigated: hardness and porosity.

Table 4 Comparison of variation of hardness after H900 and H1150 direct aging conditions. "n.d." is used when no data was found in literature

H900	H1150	Technology	Reference
+43.3%	n.d	L-PBF	[18]
+12.6%	+14.4%	L-PBF	[19]
+18.6%	n.d	L-PBF	[20]
+29.5%	n.d	L-PBF	[21]
+18.9%	−18.0%	ADAM	Current work
+52.2%	−5.0%	BMD	
+34.4%	−17.4%	FFF	

3 Results and discussion

3.1 As-sintered condition

The hardness values for all as-sintered specimens pre-H900 and pre-H1150 aging conditions are reported in Table 3, as HRC values.

The 17–4 PH processed via ADAM showed higher hardness values if compared to BMD-17–4 PH and FFF-17–4 PH, for both groups (pre-H900 and pre-H1150), and, generally, they were all close to the reference data sheet values.

The porosity analysis was then conducted according to the method reported in Sect. 2.3. The cross sections parallel to the building orientation for the three different technologies, obtained from the OM, were reported in Fig. 2. ADAM (Fig. 2a) and FFF (Fig. 2c) showed mostly triangular voids. These were more regular on the ADAM 17–4 PH specimens with respect to the FFF 17–4 PH ones, whose shape and size were more variable. These voids are defined as "air voids" or "extrusion voids" since they are conventional defects of MEX processes, caused by an incomplete adhesion between layers [13, 41]. These gaps generally occur in the green parts and remain also in the as-sintered condition. Extrusion voids were not clearly observed on the BMD 17–4 PH specimens' cross sections (Fig. 2b), where pores are smaller and more uniformly distributed.

Results obtained from the image analysis showed that porosity was comprised within 1.8% and 2.4% and there

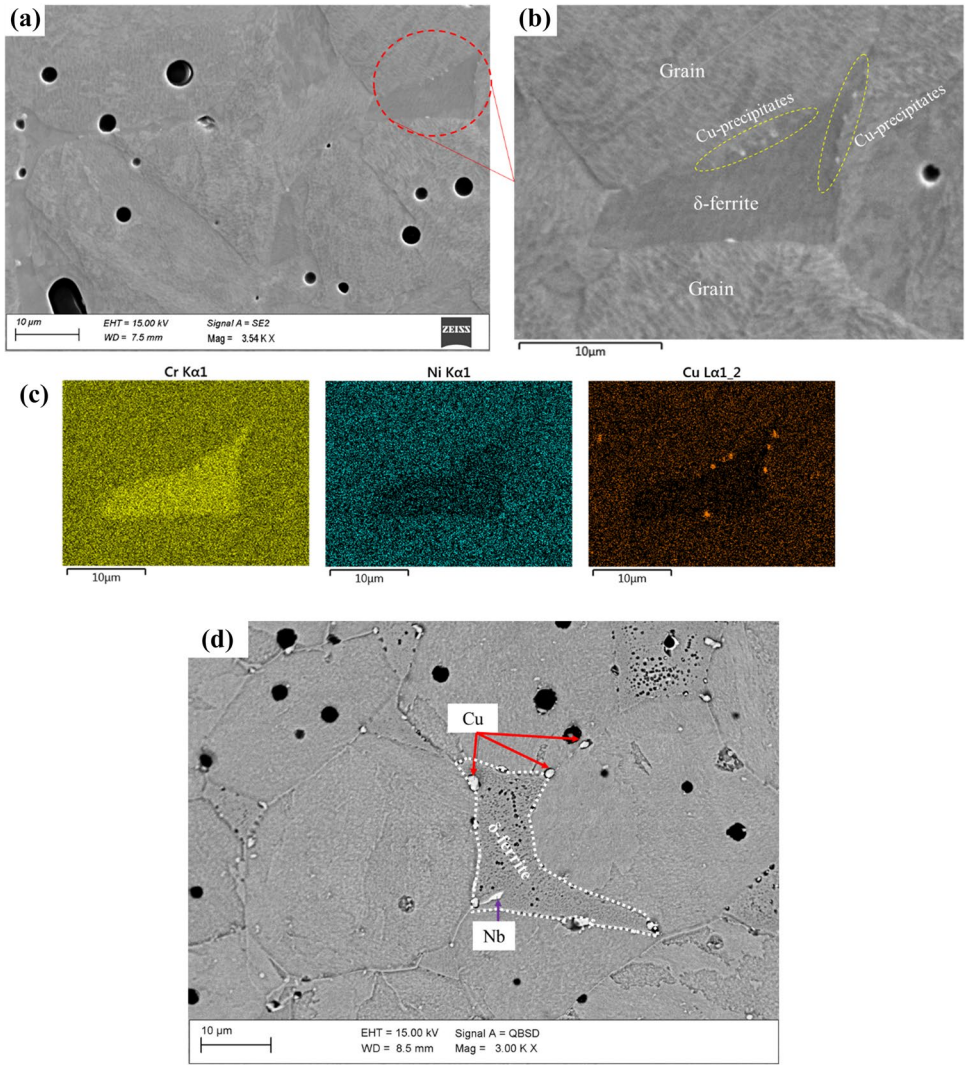

Fig. 4 BMD H900. (**a**) Overview of microstructure. (**b**) Focus on δ-ferrite and Cu-precipitates. (**c**) Chemical maps. (**d**) Cu- and Nb-precipitates along grain boundaries (etched specimen)

were not substantial differences among the technologies. More in detail, BMD registered the lowest value of porosity (1.8%) compared to FFF (2.2%) and ADAM (2.4%). From the SEM analysis conducted on the as-sintered parts, it was possible to observe the presence of equiaxial grains, inclusions of silicon oxide (SiO_2), and δ-ferrite (except for ADAM-Fig. 2a). The δ-ferrite forms at temperature above 1220 °C [42] and is detectable since it is characterized by a high content of chromium and low content of nickel and copper. The typical structure of AM 17–4 PH is composed by lath martensite and interdendritic δ-ferrite [43]. The oxides were characterized by an accumulation of oxygen and elements as silicon (Si) and a round shape.

These characteristics are in line with the literature review. Since the combination of time and temperature of sintering increases the content of oxides and δ-ferrite, as well discussed on previous study on MEX [12, 15, 32], MIM [42, 44], and BJ3DP [26, 45].

3.2 Aging treatment: H900 and H1150

After the aging treatments, new hardness tests were executed on the treated specimens, H900 and H1150. Results are reported in Fig. 3a–b and compared with the same values registered on the as-sintered specimens.

The peak-aged condition (H900) according to the standard, led to an increase of the hardness. The main cause of this effect is due to an enrichment of Cu-precipitates on the martensitic matrix during the heat treatment, as confirmed on a 17–4 PH L-PBF [21] and a 15–5 PH L-PBF [25] and on 17–4 PH commercial bars [27]. Diametrically opposite was the effect of the overaged condition (H1150), where the prolonged aging times (i.e., 4 h) and a higher treatment temperature decreased the hardness of material. More in detail, H900-treated ADAM 17–4 PH registered an average hardness value of 39.0 ± 0.2 HRC, approaching to the value of 40 HRC (the

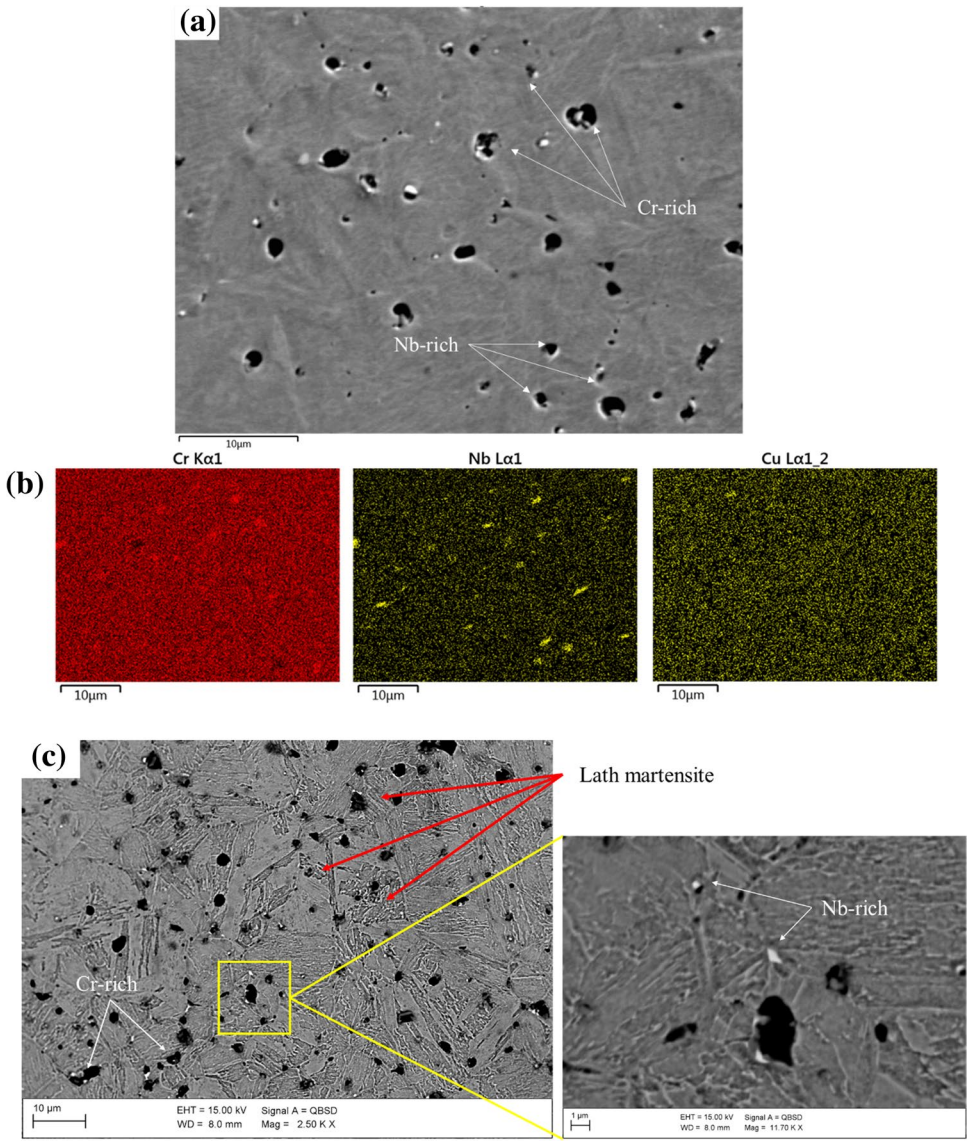

Fig. 5 ADAM H900. (**a**) Overview of microstructure. (**b**) Chemical maps. (**c**) Lath martensite, Cr- and Nb-rich precipitates (etched specimen)

minimum value from reference standard [16]) typical of a hot rolled 17–4 PH in H900 condition. BMD 17–4 PH and FFF 17–4 PH reported hardness values slightly lower, 37.1 ± 1.4 HRC and 36.5 ± 0.1 HRC, respectively. The hardness percentage increase for each investigated technology was + 18.9% for the ADAM, + 52.2% for the BMD, and 34.4% for the FFF. Comparing the obtained results to the respective data sheets, ADAM-17–4 PH H900 showed hardness values increased by 7.7% (36 HRC for ADAM-H900 data sheet [39]), while BMD-17–4 PH H900 was very close to the value of 39 HRC reported in the BMD-H900 data sheet [40]. As a general observation, the H900 heat treatment enabled an important hardness improvement of the considered specimens, and the BMD 17–4 PH showed the highest percentage increase (+ 52.2%), from 24.4 ± 0.6 HRC to 37.1 ± 1.4 HRC (Fig. 3a).

On the other hand, considering the H1150 treatment, there was a decrease of the hardness values for the three investigated technologies (Fig. 3b). BMD 17–4 PH reported the lowest percentage decrease of hardness (− 5%) from 24.3 ± 0.5 HRC to 23.1 ± 0.6 HRC. The ADAM 17–4 PH reported a percentage decrement of 18% (28.1 ± 0.8 HRC) compared to the as-sintered condition (34.3 ± 0.9 HRC) The FFF 17–4 PH H1150 showed a similar behavior compared to the ADAM 17–4 PH, with a percentage decrease of 17.4% (24.2 ± 0.9 HRC).

Despite the different feedstock used, the different debinding methods and sintering parameters, all the three technologies registered a behavior consistent with the standard after the two heat treatment conditions.

With the aim to compare the obtained results with previous works conducted on direct aged 17–4 PH stainless steel, a summary is reported in Table 4.

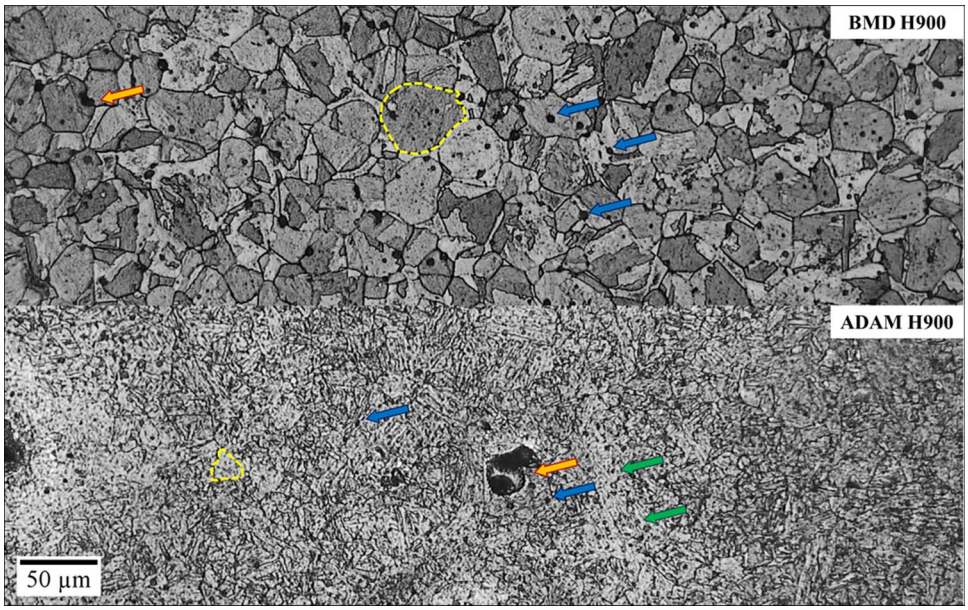

Fig. 6 Microstructure of heat-treated H900 BMD and ADAM

The percentage increase of hardness after the H900 is different for all the considered works (Table 4). This behavior can be related to the different phase composition of the material feedstock used, as reported in previous works referred to L-PBF [23]. Considering the current work, the aged H900 specimens reported substantial increments in hardness, in particular BMD 17–4 PH showed the highest increment percentage (+52.2%). As expected, this rise of hardness can be related to an increment of Cu-rich precipitates content within the matrix [25] and along the grain boundaries [22, 24], as confirmed by the SEM images (Fig. 4a–c). Figure 4 a showed the BMD 17–4 PH in H900 condition. In Fig. 4b and c, accumulations of Cu-precipitates were identified mostly along the grain boundaries. Using QBSD signal, the Cu- and Nb-rich precipitates were more visible as reported in Fig. 4d. Cu-rich reported a spherical shape, instead the Nb-rich precipitates appeared more irregular. This enrichment of precipitates caused a significant increment of hardness for BMD 17–4 PH H900. The maps of Cr, Ni, and Cu suggested also the presence of δ-ferrite in H900 condition, as already observed in the as-sintered state.

In Fig. 5a–b, the ADAM 17–4 PH H900 cross section images are reported. As for the BMD 17–4 PH H900, Cu-precipitates were detected, and also accumulations of Nb and Cr distributed in the matrix. Nb- and Cr-rich precipitates were indeed observed during the precipitation hardening on 17–4 PH stainless steel, as reported in the study of Yeli et al. [4]. The grains of ADAM 17–4 PH H900 appeared more compact because of a lower content of δ-ferrite with respect to the BMD 17–4 PH. In Fig. 5c lath martensite was recognized, as it is darker than the precipitates. The precipitates are characterized by a brighter color, and they differ also from a geometric point of view. The Nb-rich precipitates had an irregular shape and tends to form NbC, as confirmed by EDS. Instead, the Cr-rich (about 32.5 wt.%) precipitates tended to localize inside the pores, more present in the ADAM 17–4 PH specimens, as reported in Fig. 5, and to combine with O (24.4 wt.%) and Mn (14.5 wt.%), as confirmed by the EDS analyses.

Figure 6 showed the microstructures etched of BMD and ADAM in H900 condition. The ADAM H900 reported a nearly full martensitic structure with very fine grains with an average size of 24.42 ± 6.75 µm. Instead, the formation of resolved packet boundaries within the prior austenitic grain boundaries can be observed in BMD H900 [29]. A coarse grain with an average size of 41.72 ± 7.71 µm was measured. The two structures have been distinguished to the presence of δ-ferrite (SEM images-Fig. 4), the grain size, and the presence of oxides (blue arrows), larger in BMD H900 than ADAM H900. In this latter, instead, a larger size of the pores (orange arrow) and a major content of small precipitates of Cr and Nb (green arrows) were detected.

Figure 7 a–b reported the cross sections of the FFF 17–4 PH H900. As for the BMD 17–4 PH H900, the presence of δ-ferrite around grains was detected. Enrichments of Cu and Cr were also detected along the grain boundaries. Cr-rich precipitates showed in Fig. 7a were perfectly aligned and regular. Nb-rich precipitates were homogeneously dispersed within the matrix, differently from the ADAM 17–4 PH H900, where they tended to form accumulations, as it is possible to observe on the Nb map reported in Fig. 5b. Figure 7 e showed more clearly the presence of Cu precipitates

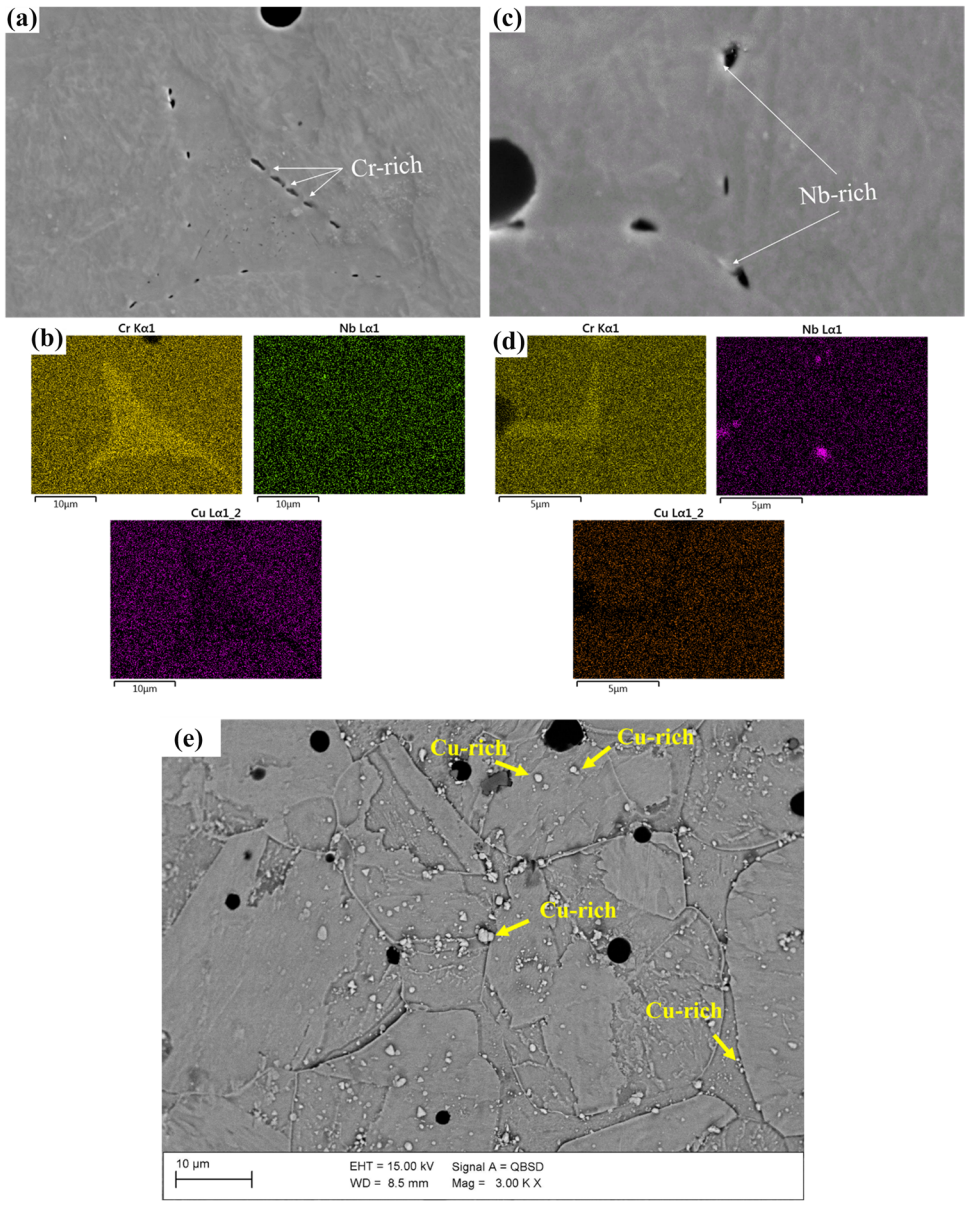

Fig. 7 FFF H900. (**a**) Overview of microstructure and Cr-rich precipitates and (**b**) its relative chemical maps. (**c**) Nb-rich precipitates and (**d**) its relative chemical map. (**e**) Cu precipitates on etched specimens

(yellow arrows) along the prior austenitic grain boundaries, inside the grains, and in areas where the δ-ferrite was present.

Moreover, it was observed that BMD 17–4 PH and FFF 17–4 PH aged at 480 °C showed more spherical inclusions (oxides or round porosity) than ADAM 17–4 PH, where they appeared irregular and larger.

Concerning the H1150, a decrease of the hardness was registered, and this tendency is confirmed by previous works about 17–4 PH [27]. In contrast, an increase of the hardness values in the overaging condition can occur [3, 19]. This behavior can be connected, in part, to the initial feedstock composition characterized by high levels of retained austenite, which tend to decrease as the aging temperature is increased [19].

More in detail, ADAM 17–4 PH and FFF 17–4 PH had a similar behaviour after the H1150 treatment, with an average decrease of 18.0% and 17.4%, respectively, while BMD 17–4 PH showed a lower decrease (5%). BMD 17–4 PH H1150 (Fig. 8) showed a high content of Cu-rich precipitates on grain boundaries and inside the matrix because of a higher temperature (620 °C) and holding time (4 h). In this condition, due to the presence of reverted austenite [28] and the coarsening of Cu-rich precipitates [20], the material became softer with respect to the other conditions (as-sintered and H900). Moreover, as observed

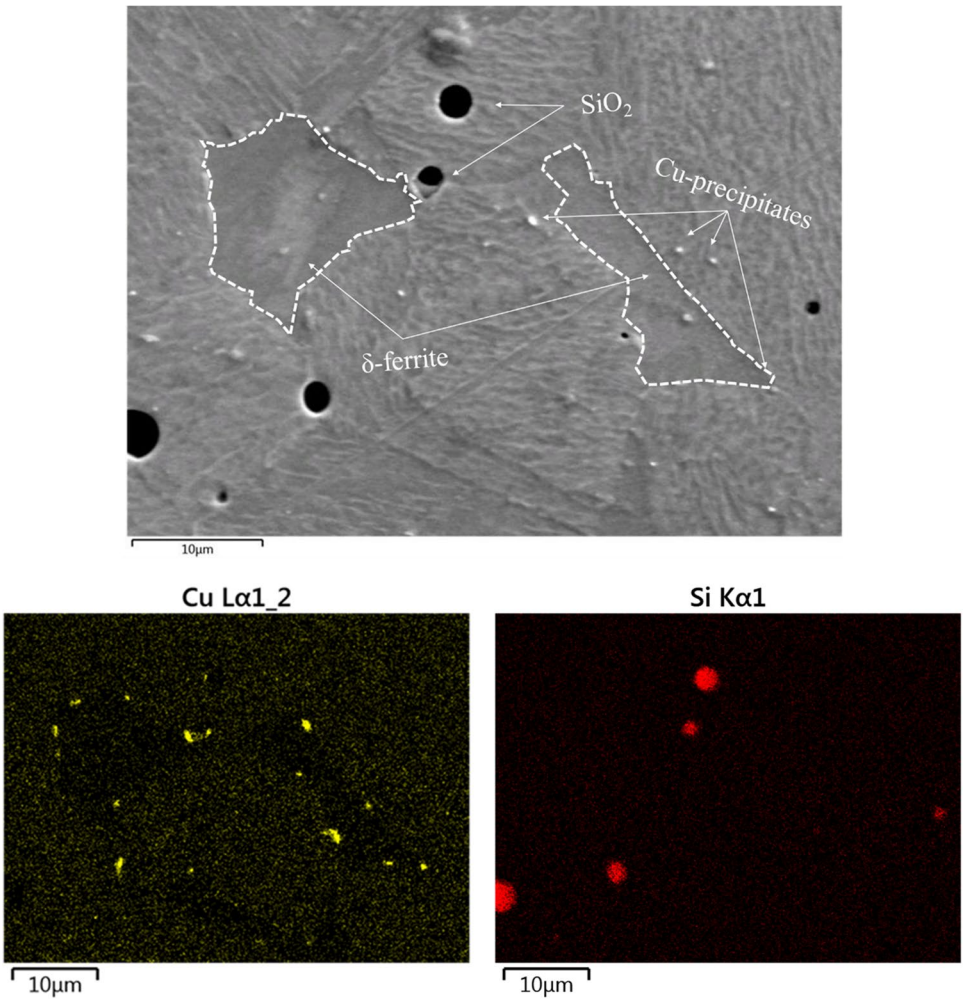

Fig. 8 Cross section of BMD H1150 and copper (Cu) and silicon (Si) map

in the Cu map (Figs. 4 and 8), levels of copper tended to decrease in correspondence of δ-ferrite zones. As reported for the as-sintered and H900 condition, BMD 17–4 PH H1150 was also characterized by round-shaped silicon oxides within the matrix.

On the other hand, ADAM 17–4 PH H1150 and FFF 17–4 PH H1150 reported a more homogeneous presence of Cu-, Nb-, and Cr-rich precipitates, as shown in Fig. 9a–b. The accumulations of Cr- and Nb- on the martensitic matrix in ADAM 17–4 PH appeared coarse and randomly dispersed, while on the FFF 17–4 PH, they were smaller and located mainly on the grain boundaries. The presence of δ-ferrite was detected among the grains for FFF 17–4 PH H1150, as for the other conditions.

From Fig. 10, the δ-ferrite was well defined in BMD H1150 and FFF H1150. In this latter, the δ-ferrite can be distinguished through a bright color, compared to the dark color of the grains. The FFF H1150 had an average size of 42.06 ± 8.75 µm, slightly lower than the H900 condition (44.76 ± 10.52 µm). For BMD H1150, the detection of the grains and their size was more difficult due to the tempered martensitic structure as observed by Huber et al. [26] on BJAM 17–4 PH-heat treated (SHT + H1150). However, an average value of 38.52 ± 9.36 µm was obtained. Also in this case, a slightly decrease was found compared to the H900 condition (41.72 ± 7.71 µm). A small content of retained austenite could be found at the grain boundaries [24, 25] of BMD H1150, but further detailed analyses are required.

Finally, the determination of porosity was executed using an optical microscope with a magnification of 140 × and the ImageJ software, for the binarization and the measurement of pores. In Fig. 11, the aged cross sections for ADAM, BMD, and FFF are shown.

Table 5 shows the average values of porosity retrieved from the image analysis and, in parenthesis, the percentage reductions with respect to the as-sintered condition.

The aging at 480 °C for 1 h allowed an important reduction of porosity for each investigated technology. The FFF specimens reported the highest reduction (− 34.3%) with an average porosity of 1.5% after treatment. The specimens realized via BMD and ADAM recorded lower percentage reductions, − 10.8% and − 18.4%, respectively. Increasing

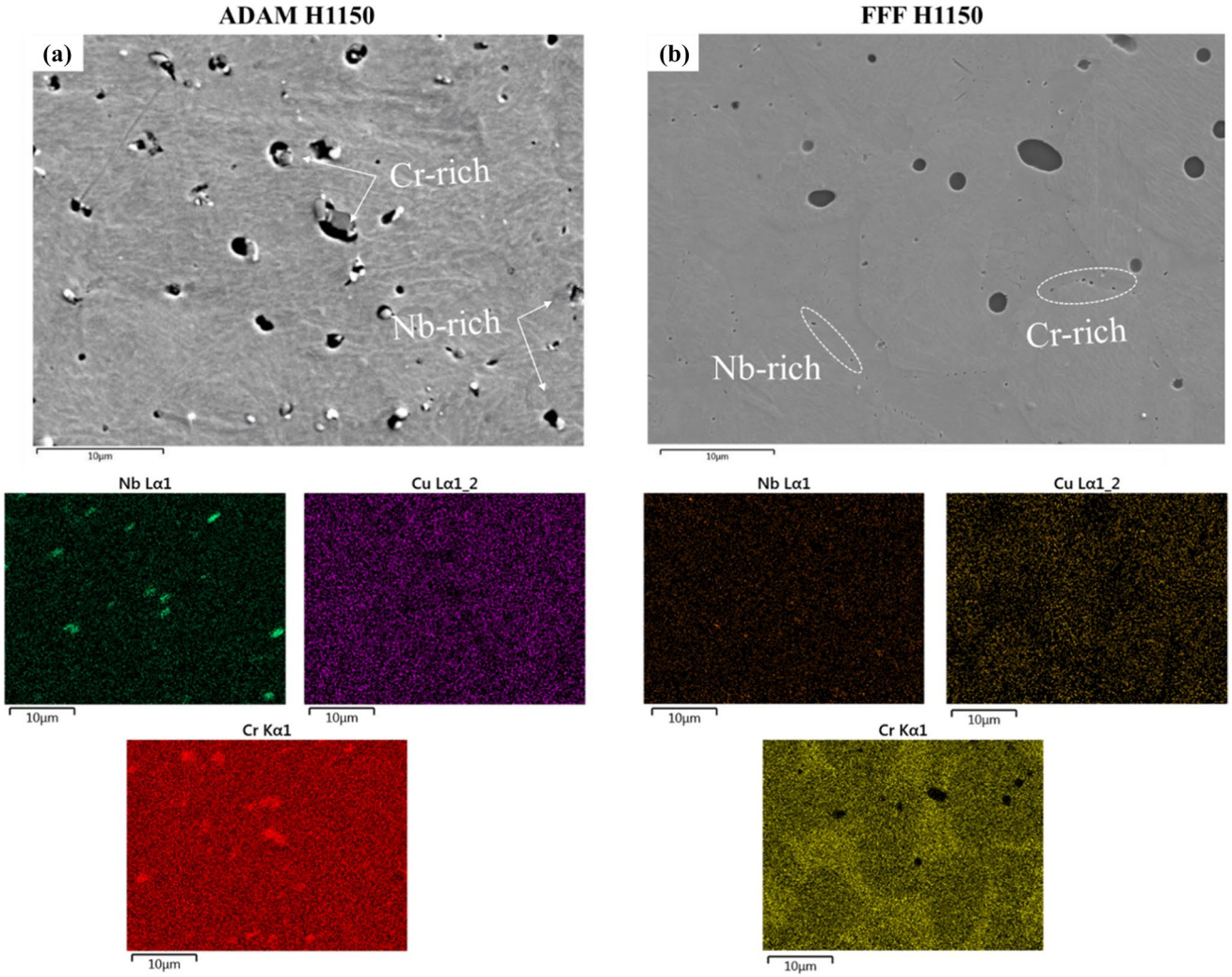

Fig. 9 (**a**) ADAM H1150 + Nb, Cu, and Cr maps. (**b**) FFF H1150 + Nb, Cu, and Cr maps

the aging temperature and holding time, 620 °C and 4 h, the maximum percentage decrease of porosity was approximately − 32.2% for ADAM 17–4 PH. The BMD and FFF 17–4 PH revealed a similar value of porosity in H1150 condition (1.8%), but the first did not register significant differences compared to the as-sintered condition, while FFF recorded a substantial decrease of porosity (− 21.3%). From the first analysis, it seemed that the specimens characterized by a high content of extrusion/air voids mostly benefited from the heat treatments (i.e., ADAM and FFF) with relevant porosity reductions. Therefore, the metal MEX technology need post-treatment on as-sintered parts to ensure the tailoring of properties with the aim to expand the applications scenario of these technologies.

In order to consolidate the results of the aging effects on hardness and porosity, a two-sample *t* test was conducted, and the *p* values obtained from the *t* test, are reported in Table 6. The null hypothesis (H_0) stated that there was no difference between the means of the as-sintered parts and the ones of the aged parts. On the contrary, the alternate hypothesis (H_1) stated that the means of the as-sintered and aged parts for the tested properties are different. A *p* value greater than 0.05 indicates that the null hypothesis is probably true.

The MEX processes considered in this work in both aging conditions, reported *p* values for the hardness lower than 0.05, so H_1 is true ($H_0 \neq H_1$). For porosity, there were sensible differences among the MEX processes and the aging conditions. The BMD 17–4 PH results, as seen in Table 5, did not report evident variation in porosity, so the null hypothesis is confirmed. Indeed, similar value in the as-sintered and H1150 conditions and a slightly decrease in the H900 condition (1.6% versus 1.8%) were recorded. On the other hand, FFF 17–4 PH, reported, in both aging conditions, a *p* value lower than 0.05, meaning that the aging affected the analyzed property. Finally,

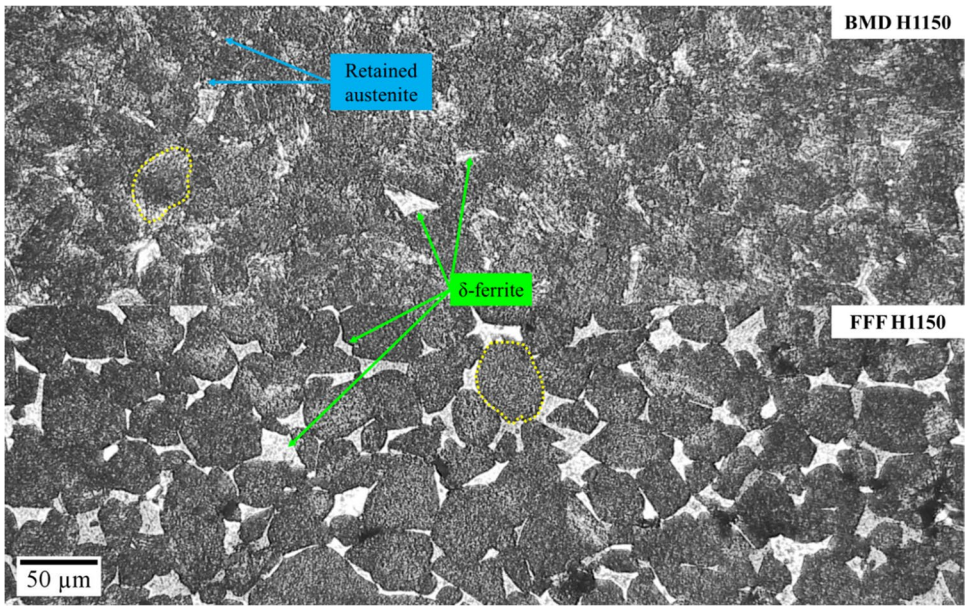

Fig. 10 Microstructure of heat-treated H1150 BMD and FFF

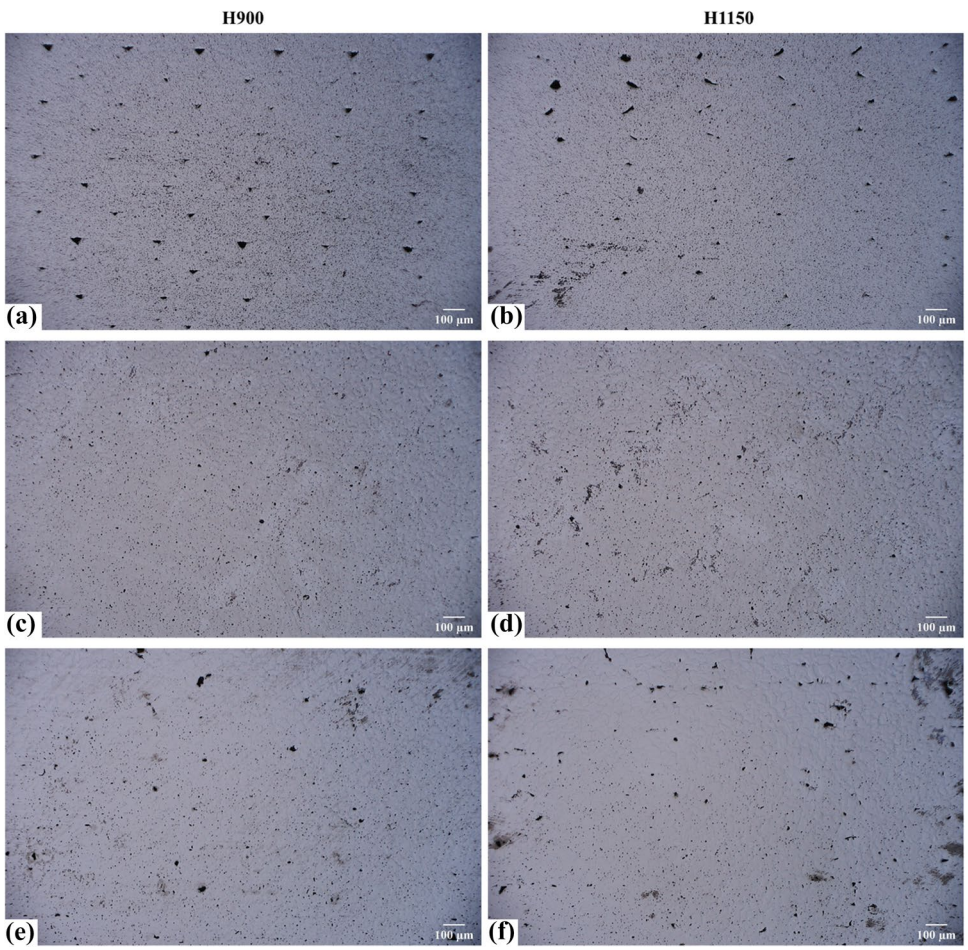

Fig. 11 Cross sections of aged specimens. (**a**) ADAM H900. (**b**) ADAM H1150. (**c**) BMD H900. (**d**) BMD H1150. (**e**) FFF H900. (**f**) FFF H1150

considering the ADAM 17–4 PH specimens, the alternative hypothesis was false (p value = 0.145) for the H900, then there was no significant effect of the treatment on porosity with respect to the as-sintered condition. While, when considering a prolonged time at a higher temperature in furnace, H1150, the influence of the heat treatment on the porosity (p value = 0.026) was significant, enabling a decrease from 2.4 to 1.6%.

Table 5 Values of porosity for different conditions of material. In parenthesis, the reduction of porosity in percentage (%)

Technology	Porosity (%)		
	As-sintered	H900	H1150
ADAM	2.4	2.0 (−18.4%)	1.6 (−32.2%)
BMD	1.8	1.6 (−10.8%)	1.8 (−1.5%)
FFF	2.2	1.5 (−34.3%)	1.8 (−21.3%)

Table 6 Results of the *t* test for the investigated properties

	Aging condition	*p* value (hardness)	*p* value (porosity)
ADAM	H900	< 0.001	0.145
	H1150	< 0.001	0.026
BMD	H900	< 0.001	0.614
	H1150	0.039	0.945
FFF	H900	< 0.001	< 0.001
	H1150	< 0.001	0.046

4 Conclusions

The present work showed the possibility to conduct heat treatments on parts made by different MEX processes, characterized by several advantages and considered an alternative to the more traditional Metal AM technologies. The results obtained allow to confirm how, despite the hybrid feedstock and D&S, the material response of MEX 17–4 PH stainless steel is similar to a hot rolled standard 17–4 PH. Thus, could be fundamental to heat treat MEX metal parts, in order to ensure a sensible modification of the properties, according to the requirements of the application fields, enhancing the hardness and the strength when necessary and reducing the porosity. Two different aging treatments were carried out, H900 and H1150. The H900 condition allowed to improve the hardness and to decrease the porosity of material, while the H1150 condition reduced the hardness and porosity.

The ADAM 17–4 PH and FFF 17–4 PH specimens seemed to be the more sensitive to heat treatments in terms of improvement of hardness and porosity, when varying aging parameters. The highest value of hardness (39.0 ± 0.2 HRC) was registered for ADAM 17–4 PH approaching the standard data (40 HRC), while the BMD 17–4 PH registered the lowest value (23.1 ± 0.6 HRC), also lower than standard data (28 HRC).

In all conditions, a decrease of porosity was observed if compared to the as-sintered state, with a maximum reduction of 34.3% (FFF 17–4 PH, H900), 32.2% (ADAM 17–4 PH, H1150), and a minimum of 1.5% (BMD 17–4 PH, H1150). Statistical analysis confirmed the significant effect of both aging treatments on the hardness values for all the involved technologies, while it showed a null effect on porosity for BMD 17–4 PH considering both, H900 and H1150, and for ADAM considering only the H900.

SEM analysis on the aged 17–4 PH specimens, allowed to detect Cu-rich, Nb-rich, and Cr-rich precipitates on the martensitic matrix (ADAM 17–4 PH) after the aging and also along the prior austenitic grain boundaries (BMD 17–4 PH and FFF 17–4 PH). The presence of precipitates can be considered the main cause of the increase of hardness in the H900 condition, while the decrease of hardness registered in the H1150 condition can be attributed to two possible effects of the overaging of 17–4 PH: the coarsening of the precipitates and a possible formation of the reverted austenite as observed in BMD H1150, but further analyses are required.

This initial study on heat-treated metal parts using these new AM processes, can encourage the research and expand the knowledge about this topic. Further analysis about the variation of mechanical properties using conventional treatments of SHT and aging, and a modelling of a thermal cycle to obtain the desired properties, where requested, will be considered.

Acknowledgements Authors want to thank CMF Marelli s.r.l., Energy Group s.r.l., and Crea 3D s.r.l for their contribution to the production of specimens and Mr. Adriano Boghetich, Prof. Pasquale Acquafredda, and Mr. Nicola Mongelli for their help to the usage of SEM.

Author contribution All authors contributed to the study conception and design. Conceptualization, material preparation, data collection, analysis, and first draft of the manuscript were performed by Alessandro Pellegrini. Methodology, writing—review, editing, and supervision were performed by Fulvio Lavecchia. Writing—review, editing, and validation were performed by Maria Grazia Guerra. Conceptualization and supervision were performed by Luigi Maria Galantucci. All authors commented on previous versions of the manuscript. All authors read and approved the final manuscript.

Funding Open access funding provided by Politecnico di Bari within the CRUI-CARE Agreement. This research received funding from the project PON "R&I" 2014–2020 ARS01_00806 "Soluzioni Innovative per la qualità e la sostenibilità dei processi di ADDitive manufacturing". This work was supported by the Italian Ministry of Education, University and Research under the Programme "Department of Excellence" Legge 232/2016 (Grant No. CUP—D94I18000260001). This research received funding from FFABR 2017, and from the project FRA 2021 "Analisi dei parametri tecnologici di Parti Realizzate in Metal FFF."

Declarations

Competing interests The authors declare no competing interests.

References

1. Vunnam S, Saboo A, Sudbrack C et al (2019) Effect of powder chemical composition on the as-built microstructure of 17–4 PH stainless steel processed by selective laser melting. Addit Manuf 30:100876. https://doi.org/10.1016/j.addma.2019.100876
2. Sung HJ, Ha TK, Ahn S et al (2002) Powder injection molding of a 17–4 PH stainless steel and the effect of sintering temperature on its microstructure and mechanical properties. J Mater Process Technol 130–131:321–327. https://doi.org/10.1016/S0924-0136(02)00739-2
3. Meredith SD, Zuback JS, Keist JS et al (2018) Impact of composition on the heat treatment response of additively manufactured 17–4 PH grade stainless steel. Mater Sci Eng A 738:44–56. https://doi.org/10.1016/j.msea.2018.09.066
4. Yeli G, Auger MA, Wilford K et al (2017) Sequential nucleation of phases in a 17–4PH steel: microstructural characterisation and mechanical properties. Acta Mater 125:38–49. https://doi.org/10.1016/j.actamat.2016.11.052
5. ISO/ASTM52900–15 (2015) Standard Terminology for additive manufacturing – general principles – terminology (ASTM52900). Int Organ Stand Geneva, Switz i:1–9
6. German RM (2018) MIM 17–4 PH stainless steel: processing, properties and best practice. Powder Inject Mould Int 12:49–76
7. Sadaf M, Bragaglia M, Nanni F (2021) A simple route for additive manufacturing of 316L stainless steel via fused filament fabrication. J Manuf Process 67:141–150. https://doi.org/10.1016/j.jmapro.2021.04.055
8. Singh G, Missiaen J, Bouvard D et al (2021) Copper extrusion 3D printing using metal injection moulding feedstock: analysis of process parameters for green density and surface roughness optimization. Addit Manuf 38:101778. https://doi.org/10.1016/j.addma.2020.101778
9. Gonzalez-Gutierrez J, Arbeiter F, Schlauf T et al (2019) Tensile properties of sintered 17–4PH stainless steel fabricated by material extrusion additive manufacturing. Mater Lett 248:165–168. https://doi.org/10.1016/j.matlet.2019.04.024
10. Godec D, Cano S, Holzer C (2020) Optimization-of-the-3D-printing-parameters-for-tensile-properties-of-specimens-produced-by-fused-filament-fabrication-of-174PH-stainless-steel2020MaterialsOpen-Access.pdf. Materials (Basel) 13:. https://doi.org/10.3390/ma13030774
11. Galati M, Minetola P (2019) Analysis of density, roughness, and accuracy of the atomic diffusion additive manufacturing (ADAM) process for metal parts. Materials (Basel) 12:. https://doi.org/10.3390/ma1224122
12. Suwanpreecha C, Seensattayawong P, Vadhanakovint V et al (2021) Influence of specimen layout on 17–4PH (AISI 630) alloys fabricated by low-cost additive manufacturing. Metall Mater Trans A Phys Metall Mater Sci 52:1999–2009. https://doi.org/10.1007/s11661-021-06211-x
13. Parenti P, Puccio D, Colosimo BM et al (2022) A new solution for assessing the printability of 17–4 PH gyroids produced via extrusion-based metal AM. J Manuf Process 74:557–572. https://doi.org/10.1016/j.jmapro.2021.12.043
14. Watson A, Belding J, Ellis BD (2020) Characterization of 17–4 PH processed via bound metal deposition (BMD). Miner Met Mater Ser 205–216. https://doi.org/10.1007/978-3-030-36296-6_19
15. Lavecchia F, Pellegrini A, Galantucci LM (2023) Comparative study on the properties of 17–4 PH stainless steel parts made by metal fused filament fabrication process and atomic diffusion additive manufacturing. Rapid Prototyp J 29:393–407. https://doi.org/10.1108/RPJ-12-2021-0350
16. ASTM International (2013) Standard specification for hot-rolled and cold-finished age-hardening stainless steel. 1–8. https://doi.org/10.1520/A0564
17. Pasebani S, Ghayoor M, Badwe S et al (2018) Effects of atomizing media and post processing on mechanical properties of 17–4 PH stainless steel manufactured via selective laser melting. Addit Manuf 22:127–137. https://doi.org/10.1016/j.addma.2018.05.011
18. Murr LE, Martinez E, Hernandez J et al (2012) Microstructures and properties of 17–4 PH stainless steel fabricated by selective laser melting. J Mater Res Technol 1:167–177. https://doi.org/10.1016/S2238-7854(12)70029-7
19. LeBrun T, Nakamoto T, Horikawa K et al (2015) Effect of retained austenite on subsequent thermal processing and resultant mechanical properties of selective laser melted 17–4 PH stainless steel. Mater Des 81:44–53. https://doi.org/10.1016/j.matdes.2015.05.026
20. Sabooni S, Chabok A, Feng SC et al (2021) Laser powder bed fusion of 17–4 PH stainless steel: a comparative study on the effect of heat treatment on the microstructure evolution and mechanical properties. Addit Manuf 46:102176. https://doi.org/10.1016/j.addma.2021.102176
21. Hsu TH, Chang YJ, Huang CY et al (2019) Microstructure and property of a selective laser melting process induced oxide dispersion strengthened 17–4 PH stainless steel. J Alloys Compd 803:30–41. https://doi.org/10.1016/j.jallcom.2019.06.289
22. Nezhadfar PD, Shrestha R, Phan N et al (2019) Fatigue behavior of additively manufactured 17–4 PH stainless steel: synergistic effects of surface roughness and heat treatment. Int J Fatigue 124:188–204. https://doi.org/10.1016/j.ijfatigue.2019.02.039
23. Shaffer DJ, Wilson-Heid AE, Keist JS et al (2021) Impact of retained austenite on the aging response of additively manufactured 17–4 PH grade stainless steel. Mater Sci Eng A 817:141363. https://doi.org/10.1016/j.msea.2021.141363
24. Zhou T, Zheng T, Yildiz AB, et al (2022) Microstructure control during deposition and post-treatment to optimize mechanical properties of wire-arc additively manufactured 17–4 PH stainless steel. Addit Manuf 58:. https://doi.org/10.1016/j.addma.2022.103047
25. Chae H, Luo MY, Huang EW et al (2022) Unearthing principal strengthening factors tuning the additive manufactured 15–5 PH stainless steel. Mater Charact 184:111645. https://doi.org/10.1016/j.matchar.2021.111645
26. Huber D, Stich P, Fischer A (2021) Heat treatment of 17–4 PH stainless steel produced by binder jet additive manufacturing (BJAM) from N2-atomized powder. Prog Addit Manuf. https://doi.org/10.1007/s40964-021-00224-z
27. Hsiao CN, Chiou CS, Yang JR (2002) Aging reactions in a 17–4 PH stainless steel. Mater Chem Phys 74:134–142. https://doi.org/10.1016/S0254-0584(01)00460-6
28. Viswanathan UK, Banerjee S, Krishnan R (1988) Effects of aging on the microstructure of 17–4 PH stainless steel. Mater Sci Eng 104:181–189. https://doi.org/10.1016/0025-5416(88)90420-X
29. Sathyanath A, Meena A (2022) Microstructure-induced high-strain-rate deformation behavior of heat-treated 17–4 PH stainless steel. J Mater Eng Perform. https://doi.org/10.1007/s11665-022-07065-z

30. Condruz MR, Paraschiv A, Puscasu C (2018) Heat treatment influence on hardness and microstructure of ADAM manufactured 17–4 Ph. Turbo V:4–11
31. Bouaziz MA, Djouda JM, Chemkhi M et al (2021) Heat treatment effect on 17–4PH stainless steel manufactured by atomic diffusion additive manufacturing (ADAM). Procedia CIRP 104:935–938. https://doi.org/10.1016/j.procir.2021.11.157
32. Abe Y, Kurose T, Santos MVA et al (2021) Effect of layer directions on internal structures and tensile properties of 17–4ph stainless steel parts fabricated by fused deposition of metals. Materials (Basel) 14:1–12. https://doi.org/10.3390/ma14020243
33. Galantucci LM, Guerra MG, Dassisti M et al (2019) Additive manufacturing: new trends in the 4th Industrial Revolution. Springer International Publishing. https://doi.org/10.1007/978-3-030-18180-2_12
34. Gabilondo M, Cearsolo X, Arrue M, et al (2022) Influence of build orientation, chamber temperature and infill pattern on mechanical properties of 316L Parts Manufactured by Bound Metal Deposition. Materials (Basel) 15:. https://doi.org/10.3390/ma15031183
35. Enrique PD, DiGiovanni C, Mao N et al (2021) Resistance is not futile: the use of projections for resistance joining of metal additively and conventionally manufactured parts. J Manuf Process 66:424–434. https://doi.org/10.1016/j.jmapro.2021.04.035
36. Pellegrini A, Palmieri ME, Guerra MG (2022) Evaluation of anisotropic mechanical behaviour of 316L parts realized by metal fused filament fabrication using digital image correlation. Int J Adv Manuf Technol. https://doi.org/10.1007/s00170-022-09303-z
37. BASF 3D Printing Solutions (2021) BASF Ultrafuse 17–4 PH. https://www.sculpteo.com/en/materials/fdm-material/ultrafuse-17-4-ph/. Accessed 13 Dec 2021
38. Pottery G, Mangone A, Caggiani MC, et al (2023) A possible natural and inexpensive substitute for lapis lazuli in the Frederick II era: the finding of haüyne in blue lead-tin. Molecules 28:. 10.3390/ molecules28041546
39. Markforged (2018) 17–4 PH stainless steel. https://markforged.com/materials/metals/17-4-ph-stainless-steel. Accessed 22 Apr 2021
40. Desktop Metal Inc. (2021) 17–4PH-stainless-steel. https://www.desktopmetal.com/uploads/BMD-SPC-MDS-17-4ph-211112_c.pdf. Accessed 21 Jan 2022
41. Singh G, Missiaen JM, Bouvard D, et al (2021) Additive manufacturing of 17–4 PH steel using metal injection molding feedstock: analysis of 3d extrusion printing, debinding and sintering. addit manuf 47:. https://doi.org/10.1016/j.addma.2021.102287
42. Wu Y, German RM, Blaine D et al (2002) Effects of residual carbon content on sintering shrinkage, microstructure and mechanical properties of injection molded 17–4 PH. J Mater Sci 37:3573–3583. https://doi.org/10.1023/A:1016532418920
43. Caballero A, Ding J, Ganguly S et al (2019) Wire + arc additive manufacture of 17–4 PH stainless steel: effect of different processing conditions on microstructure, hardness, and tensile strength. J Mater Process Technol 268:54–62. https://doi.org/10.1016/j.jmatprotec.2019.01.007
44. Wu MW, Huang ZK, Tseng CF et al (2015) Microstructures, mechanical properties, and fracture behaviors of metal-injection molded 17–4PH stainless steel. Met Mater Int 21:531–537. https://doi.org/10.1007/s12540-015-4369-y
45. Huber D, Vogel L, Fischer A (2021) The effects of sintering temperature and hold time on densification, mechanical properties and microstructural characteristics of binder jet 3D printed 17–4 PH stainless steel. Addit Manuf 46:102114. https://doi.org/10.1016/j.addma.2021.102114